

Lateral velocity distribution in open channels with partially flexible submerged vegetation

Lijuan Han¹ · Yuhong Zeng¹ · Li Chen¹ · Wenxin Huai¹

Received: 28 May 2015 / Accepted: 21 September 2016 / Published online: 4 October 2016
© Springer Science+Business Media Dordrecht 2016

Abstract This study implemented three analytical models to investigate the lateral distribution of depth-averaged streamwise velocity in a rectangular channel with lateral, unevenly-distributed, flexible submerged vegetation. Secondary flow, vegetation drag, and turbulent shear were introduced into the momentum equations to represent the interaction between vegetation and flow. Comparison of model results and experimental data indicated that predictions were improved with a mixing layer model, which considers the secondary flow term in the mixing region, particularly for channels with a high aspect ratio. The research established a relationship between the vegetation drag coefficient and the Reynolds number. A sensitivity analysis of the dimensionless eddy viscosity coefficient and bed friction factor indicated that the coefficient had as significant an impact as the second factor on the lateral velocity profile. A reasonable dimensionless eddy viscosity coefficient is essential to predict velocity accurately.

Keywords Lateral velocity distribution · Submerged vegetation · Secondary flow · Mixing region · Sensitivity analysis

1 Introduction

In nature, aquatic vegetation grows heterogeneously. Riparian vegetation may be present in simple or compound channels, and profoundly influences flow characteristics within vegetative and non-vegetative zones. The vegetation in channels affects local water depth and velocity profile, meanwhile, these influence on flow vary with vegetation type and distribution. Generally, streamwise velocity is fast in the non-vegetated zone, and slows in the

✉ Yuhong Zeng
yhzeng@whu.edu.cn

¹ State Key Laboratory of Water Resources and Hydropower Engineering Science, Wuhan University, Wuhan 430072, People's Republic of China

vegetated zone. The velocity gradient between the vegetated and non-vegetated zones leads to a mass and momentum exchange with secondary circulations. This region is called the mixing region or mixing layer [1]. Previous research demonstrated that local water depth, secondary flow intensity, turbulence, and vegetation drag force affect velocity profile [2–7].

The lateral profile of velocity provides an approximate view of discharge and solute transport features; these profiles have interested many researchers. Shiono and Knight [2–4] presented an analytical model of compound channels to predict the lateral velocity distribution and bed shear stress, dividing the channels into several subsections. This approach is known as the Shiono and Knight Method (SKM), and since its publication, the SKM has been continuously improved to improve specific predictions.

Ervine et al. [5] introduced a secondary flow term to the SKM model, to estimate the velocity and shear stress for straight and meandering overbank flow patterns. This approach emphasized the secondary flow term in rectangular prismatic channels. Subsequent research demonstrated that the secondary cells significantly influence velocity distribution [6, 7]. Van Prooijen et al. [8] proposed a new eddy viscosity model, incorporating the horizontal coherent structures and the bottom turbulence to quantify the transverse momentum exchange. Tang et al. [9] presented a new boundary condition at the interface between the main channel and the adjoined floodplain, effectively predicting the lateral velocity distribution.

Other investigations have analyzed channel flow characteristics by dividing channels with emergent vegetation into several subsections [10–14]. Rameshwaran et al. [10] proposed a quasi, two-dimensional model to calculate the depth-averaged velocity and bed shear stress in a prismatic channel with emergent vegetated floodplain. This study also introduced vegetation drag term and porosity factor to represent the effect of vegetation. Huai et al. [11, 12] developed a lateral profile of streamwise velocity in a compound and rectangular channel with partially emergent artificial rigid vegetation. Chen et al. [13] solved depth-averaged velocity by solving the dimensionless momentum equation; this expression establishes a relationship between the secondary flow and the inertia. In a related study, de Lima et al. [14] analyzed the linear stability of the lateral velocity gradient in a channel with partial vegetation. Liu et al. [15] introduced porosity to represent the effect of vegetation in the SKM; the new model has been used to predict depth-averaged velocity and bed shear stress successfully in a compound channel with emergent and submerged vegetation.

Although these different models have predicted the lateral velocity distribution in an open channel with lateral unevenly distributed vegetation, most have focused on compound channels with rigid emergent vegetation on the floodplain. However, flexible submerged vegetation is common in rivers, and corresponding analytical models for lateral velocity are rare. In addition, the role of secondary flow on the prediction precision is unclear, and the parameters in corresponding models need to be defined.

This study compared different models predicting the lateral profile of streamwise velocity in a rectangular channel with partially covered flexible submerged vegetation. Further, laboratory experiments were conducted to calibrate model parameters, including the secondary flow coefficient, dimensionless eddy viscosity, vegetation drag coefficient, and the bed friction factor.

2 Theoretical analysis

This study focuses on the transverse distribution of depth-averaged longitudinal velocity in a rectangular open channel with partially flexible submerged vegetation (Fig. 1). In this figure, H is the flow depth, h_v is the height of vegetation, B is the channel width, B_{nv} and B_v

is the width of non-vegetated and vegetated zones, respectively (subscript nv and v are used to identify parameters in non-vegetated and vegetated zones).

Based on mechanical analysis results, the governing equation representing the longitudinal motion of a fluid element in a steady uniform flow is:

$$\rho g S_0 dx dy dz + \frac{\partial \tau_{zx}}{\partial z} dx dy dz + \frac{\partial \tau_{yx}}{\partial y} dx dy dz - \frac{1}{2} \rho C_D \lambda u_v^2 dx dy dz = \frac{\partial \rho u v}{\partial y} dx dy dz \quad (1)$$

In this equation, ρ is the fluid density; g is the gravitational acceleration; S_0 is the channel slope; τ is the Reynolds stress in corresponding panels; C_D is the plant drag coefficient (in the non-vegetated zone $C_D = 0$). Further, λ is the density of vegetation; it is defined as $\lambda = \alpha m D$, where m is the number of branches per unit channel area; D is the branch diameter; and α is a constant reflecting the projected area ratio of stem-leaf to stem. In other words, α is the total projected area of stem-leaf divided by the projected area of stem. Additionally, u_v is the local mean streamwise velocity around the vegetation; u and v are local mean velocity components corresponding to x and y ; x, y, z are longitudinal, lateral, and vertical coordinates.

Equation (1) does not consider vegetation blockage, since the porosity of the vegetative is high. Liu et al. [15] demonstrated that in these cases, the influence of porosity on the lateral distribution of streamwise velocity can be ignored.

By integrating Eq. (1) over the water depth H , the depth-averaged equation is obtained:

$$\rho g S_0 H - \tau_b + \int_{z(y)}^H \frac{\partial \tau_{yx}}{\partial y} dz - \frac{1}{2} \rho C_D \lambda h_v U_v^2 = \frac{\partial \rho H (uv)_d}{\partial y} \quad (2)$$

In this expression, U_v is the depth-averaged velocity around the vegetation; subscript d is the depth-averaged value; τ_b is the bed shear stress; and the right hand term presents the lateral gradient of the secondary flow [5], and $z_{(y)} = \begin{cases} 0, & 0 \leq y \leq B_{nv} \\ h_v, & B_{nv} < y \leq B \end{cases}$.

To obtain the depth-averaged streamwise velocity U_d in channels with submerged vegetation, Stone and Shen [16] introduced the submergence degree coefficient h^*

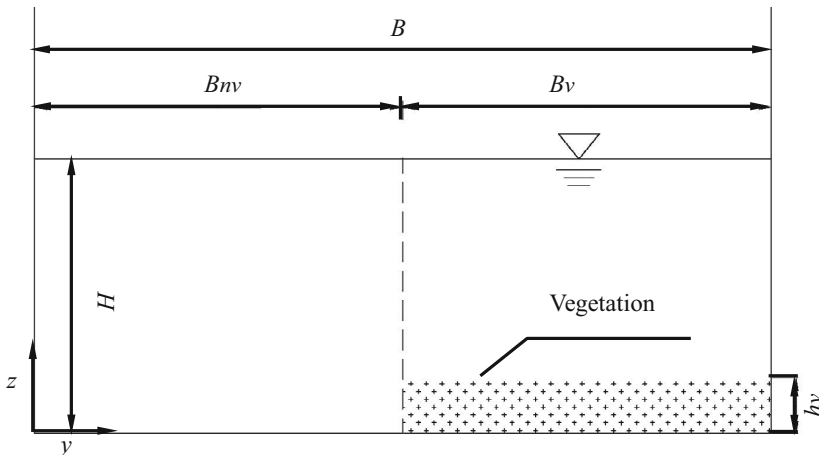


Fig. 1 Sketch of open channel with partial vegetation

($h^* = h_v/H$). They further established the relationship between U_v and U_d , as $U_v/U_d = \sqrt{h^*k_v}$, where $k_v = [(1 - Dm^{0.5})/(1 - h^*Dm^{0.5})]^2$. However, this expression was developed for rigid cylinders, and it does not apply to the flexible vegetation in this experiment. As such, we introduced the coefficient η to estimate the ratio of U_v to U_d . This study also introduced the depth-averaged lateral shear stress $\overline{\tau_{yx}}$, Darcy-Weisbach friction factor f , the depth-averaged eddy viscosity ϵ_{yx} , a dimensionless eddy viscosity ζ , and the local shear velocity U^* . These are expressed, respectively, as:

$$\overline{\tau_{yx}} = \frac{1}{H} \int_{z(y)}^{z_s} \tau_{yx} dz, \quad f = \frac{8\tau_b}{\rho U_d^2}, \quad \overline{\tau_{yx}} = \rho \epsilon_{yx} \frac{dU_d}{dy}, \quad \epsilon_{yx} = \zeta H U^* = \zeta H U_d \sqrt{f/8}$$

Secondary flows cannot be ignored in natural channels, particularly those that are partially vegetated [5, 7, 15]. Ervine et al. [5] expressed the secondary flow term as $(uv)_d = k_1 \cdot k_2 U_d^2 = K U_d^2$, where K was assumed to be a constant to represent the intensity of secondary flow cells in a compound channel. In real-world conditions, u and v vary with z ; as such, k_1 and k_2 also vary with z , so K is not a constant along the z direction. The sign of secondary current term should be determined from the location and rotation of the secondary current cells. Spooner and Shiono [17] also demonstrated that K was not constant across a strong secondary flow in a meandering channel. In the paper, an analytical solution was given by assuming $(uv)_d = \overline{K} U_d^2$ (Eq. 3), though \overline{K} was alterable across a secondary cell [17]. Consistent with Tang et al. [7] and Liu et al. [15], $(uv)_d$ can be expressed as:

$$(uv)_d = \frac{1}{H} \int_0^H (uv) dz = \frac{1}{H} \int_0^H (k_1(z)k_2(z)U_d^2) dz = U_d^2 \frac{1}{H} \int_0^H (k_1(z)k_2(z)) dz = \overline{K} U_d^2 \quad (3)$$

In this expression, \overline{K} is a depth-averaged value, and should vary from positive (clockwise cell) to negative (anti-clockwise cell), depending on the secondary flow cell rotation. Equation (2) can be expressed as a second-order linear ordinary differential equation using U_d :

$$\rho g S_0 H - \frac{f}{8} \rho U_d^2 + \frac{\partial}{\partial y} \left\{ \rho \zeta H^2 \left(\frac{f}{8} \right)^{1/2} U_d \frac{\partial U_d}{\partial y} - \rho H \overline{K} U_d^2 \right\} - \frac{1}{2} \rho C_D \lambda h_v \eta^2 U_d^2 = 0 \quad (4)$$

This model is called a secondary flow model (SFM); the analytical solution for Eq. (4) is

$$\begin{cases} (U_d)_{nv} = \left(C_1 e^{r_1 y} + C_2 e^{r_2 y} + \frac{g S_0 H}{f/8} \right)^{1/2} \\ (U_d)_v = \left(C_3 e^{r_3 y} + C_4 e^{r_4 y} + \frac{g S_0 H}{f/8 + C_D \lambda h_v \eta^2 / 2} \right)^{1/2} \end{cases} \quad (5)$$

where $r_{1,2} = \frac{\overline{K}_{nv} \pm \sqrt{\overline{K}_{nv}^2 + \zeta_m \left(\frac{f}{8}\right)^{1/2} (f/4)}}{\zeta_m H \left(\frac{f}{8}\right)^{1/2}}, r_{3,4} = \frac{\overline{K}_v \pm \sqrt{\overline{K}_v^2 + \zeta_v \left(\frac{f}{8}\right)^{1/2} [C_D \lambda h_v \eta^2 + f/4]}}{\zeta_v H \left(\frac{f}{8}\right)^{1/2}}$.

When $\overline{K} = 0$, Eq. (4) is the same form as presented by Huai et al. [11]; it ignores the effect of secondary flow. We call this the Huai Model (HM). In this model, we divide the channel into 2 sub-regions, the non-vegetated and vegetated regions, respectively:

$$\rho g S_0 H - \frac{f}{8} \rho U_d^2 + \frac{\partial}{\partial y} \left\{ \rho \zeta H^2 \left(\frac{f}{8} \right)^{1/2} U_d \frac{\partial U_d}{\partial y} \right\} - \frac{1}{2} \rho C_D \lambda h_v \eta^2 U_d^2 = 0 \tag{6}$$

By solving Eq. (6), the depth-averaged velocity U_d is given by:

$$\begin{cases} (U_d)_{nv} = \left(C_1 e^{r_1 y} + C_2 e^{-r_1 y} + \frac{g S_0 H}{f/8} \right)^{1/2} \\ (U_d)_v = \left(C_3 e^{r_2 y} + C_4 e^{-r_2 y} + \frac{g S_0 H}{f/8 + C_D \lambda h_v \eta^2 / 2} \right)^{1/2} \end{cases} \tag{7}$$

Within this expression, $r_1 = \sqrt{\frac{2}{\zeta_{nv}} \left(\frac{f}{8} \right)^{1/4} \frac{1}{H}}$, $r_2 = \sqrt{\frac{f/8 + C_D \lambda h_v \eta^2 / 2}{\zeta_v H^2 (f/8)^{1/2} / 2}}$.

According to van Prooijen et al. [8], a compound channel’s cross-section can be divided into two laterally uniform regions and a mixing region. An intense transverse exchange of mass and momentum occurs at the mixing region (see Fig. 1 in [8]). In this study, we adopt this mixing region concept; the mass transport and increased momentum are assumed to occur primarily in the mixing layer. The corresponding model is called the mixing layer model (MLM). Laboratory measurements show that the mixing layer width is approximately 10 % of the channel width, and the layer is mainly located on the non-vegetated side.

The mixing layer width, δ , is defined according to van Prooijen et al. [8] as $\delta = 2(y_{75\%} - y_{25\%})$. The cross section is then divided into four areas: the non-vegetated region, the mixing layer in the non-vegetated region, the mixing layer in vegetated region, and the vegetated region. To solve the second-order linear ordinary differential equation, U_d is expressed as:

$$\begin{cases} U_{d1} = \left(C_1 e^{r_1 y} + C_2 e^{r_2 y} + \frac{8gS_0H}{f} \right)^{1/2} \\ U_{d2} = \left(C_3 e^{r_3 y} + C_4 e^{r_4 y} + \frac{8gS_0H}{f} \right)^{1/2} \\ U_{d3} = \left(C_5 e^{r_5 y} + C_6 e^{r_6 y} + \frac{gS_0H}{f/8 + C_D \lambda h_v \eta^2 / 2} \right)^{1/2} \\ U_{d4} = \left(C_7 e^{r_7 y} + C_8 e^{r_8 y} + \frac{gS_0H}{f/8 + C_D \lambda h_v \eta^2 / 2} \right)^{1/2} \end{cases} \tag{8}$$

In this expression, $r_{1,2} = \pm \sqrt{\frac{2}{\zeta_{nv}} \left(\frac{f}{8} \right)^{1/4} \frac{1}{H}}$, $r_{3,4} = \frac{\bar{K}_2 \pm \sqrt{\bar{K}_2^2 + \zeta_{nv} \left(\frac{f}{8} \right)^{1/2} (f/4)}}{\zeta_{nv} H \left(\frac{f}{8} \right)^{1/2}}$,

$$r_{5,6} = \frac{\bar{K}_3 \pm \sqrt{\bar{K}_3^2 + \zeta_v \left(\frac{f}{8} \right)^{1/2} (C_D \lambda h_v \eta^2 + f/4)}}{\zeta_v H \left(\frac{f}{8} \right)^{1/2}}$$
, $r_{7,8} = \pm \sqrt{\frac{f/8 + C_D \lambda h_v \eta^2 / 2}{\zeta_v H^2 (f/8)^{1/2} / 2}}$.

Assuming that each domain’s flow is unaffected by adjacent domains, the unknown coefficient C_i is determined by solving the linear equations using the Gaussian elimination method [18]. The boundary conditions are:

1. No-slip condition, i.e. $U_d = 0$ at the edge of the channel;
2. At the interface between two zones, we applied the continuity of unit force proposed by Tang et al. [9]:

$$(H\overline{\tau_{xy}})_{y=0.3}^{(i)} + h\tau_m = (H\overline{\tau_{xy}})_{y=0.3}^{(i+1)}, \quad \tau_m = \frac{1}{8}\rho f_m U_d^2 \quad (9)$$

In this expression, f_m is the mean value of f_{nv} and f_v .

3. Continuity of velocity at the joint of panels, i.e., $(U_d)_i = (U_d)_{i+1}$, $\partial(U_d)_i/\partial y = \partial(U_d)_{i+1}/\partial y$.

3 Determining model parameters

Before using the models above to form predictions, it was important to determine values for f , ζ , \overline{K} , C_D and λ . In general, reasonable values for these parameters are obtained using curve fitting techniques, based on experiments, experience [19, 20], or a multi-objective evolutionary algorithm [21].

3.1 Darcy-Weisbach factor f

Significant research has been conducted about f [2, 22, 23]; these can significantly influence prediction accuracy [24]. In this study, f was obtained using the equation $f = 8gn^2/R^{1/3}$, where R is the hydraulic radius for each subarea. Preliminary tests were conducted in the experimental channel, without vegetation, to derive the Manning's coefficient n . As such, the friction factor f is the "skin friction" of the bed surface and does not account for the resistance to flow caused by vegetation. Although f is affected by secondary flow and bottom turbulence in the mixing layer, the lateral variation of f is not accounted for.

3.2 Dimensionless eddy viscosity coefficient

Researchers have also proposed different expressions of eddy viscosity to estimate transverse momentum [4, 8, 25, 26]. For non-vegetated regions, past research has reported dimensionless eddy viscosity coefficients varying from 0.08 to 0.4 [7, 23, 24, 27, 28]. Here, the dimensionless eddy viscosity coefficients, ζ_{nv} and ζ_v , were the average values of that in the non-vegetated and vegetated regions. These were obtained indirectly from the Reynolds stress values, based on the measured turbulent velocities.

3.3 Parameter \overline{K}

The parameter \overline{K} is a proportional factor that varies along the cross-section to characterize secondary flow intensity. Flow characteristics over vegetation vary with local water depth, and the intensity and number of secondary flow cells change simultaneously. Besides, the sign of \overline{K} is determined by the rotation of secondary current cells, and the accuracy of prediction is related to the number of secondary cells. Therefore, different values of \overline{K} are needed to reflect secondary cell intensity.

With respect to the models considered above, the HM model ignores secondary flow (i.e. $\overline{K} = 0$), whereas SFM and MLM determine \overline{K} values using the trial-and-error method; values vary from -0.024 to 0.006 .

3.4 Vegetation resistance

The drag force on flexible vegetation differs from the drag force on rigid vegetation, because of vegetation deformation and reorganization. Many studies [20, 29–31] have characterized flow resistance, but this parameter often relies on study of specific vegetation, and cannot be easily extrapolated to other studies. For natural reeds with foliage, larger values of C_D are reported [29, 32, 33].

Vegetation resistance is not only related to the vegetation drag coefficient C_D , but also to the vegetation density λ . For our experiments, the vegetation density λ was static, based on the expression $\lambda = \alpha mD$; the value of α was as 1.25, based on the projected area ratio of stem-leaf to stem. Therefore, the value of λ is 2.5 m^{-1} , and vegetation resistance variance was represented by the varying drag coefficient C_D . In this study, a trial-and-error method was used to obtain C_D , providing a best fit with the depth-averaged velocity data.

4 Laboratory experiment

A 0.6 m wide and 20 m long glass rectangular channel in the Hydraulic Laboratory of Wuhan University in China was adopted for experiment. The bed slope S_0 was fixed at 0.04 %. Plastic artificial grass with a height of 4.5 cm (Fig. 2) covered half of the channel; each grass plant consisted of four branches of approximately 1 mm diameter (i.e. $D = 1 \text{ mm}$), each with six leaves. The grass was positioned in a parallel pattern at a density of $2000 \text{ stems m}^{-2}$ (m). The channel's flow discharge was controlled by an electric magnetic valve with an accuracy of 0.1 L s^{-1} ; a downstream gate was adjusted to ensure uniformity of flow.

In this study, seven cases were conducted; Table 1 lists the corresponding hydraulic parameters, and η was obtained based on the measured values for U_v and U_d . Terms are defined as follows: H_r is the relative depth ($H_r = (H - h_v)/H$), β is the aspect ratio ($\beta = B/$



Fig. 2 Experimental set up

Table 1 Experimental cases

Cases	Q (L s ⁻¹)	H (cm)	H_r	β	η	U_{cv} (m s ⁻¹)	Re_v
A1	20.0	16.0	0.72	3.75	0.73	0.104	99.39
A2	30.0	18.0	0.75	3.33	0.59	0.164	156.73
B1	16.5	13.6	0.67	4.41	0.73	0.091	86.96
B2	19.5	12.6	0.64	4.76	0.77	0.111	106.08
B3	16.0	19.0	0.76	3.16	0.81	0.070	66.90
B4	10.0	11.6	0.61	5.17	0.82	0.049	46.83
B5	14.9	14.6	0.69	4.20	0.81	0.074	70.72

H), and Re_v is the Reynolds number in the vegetation region ($Re_v = \alpha DU_{cv}/\nu$). In this final parameter, U_{cv} is the temporally and cross-sectionally averaged velocity in the vegetated zone, and ν is the kinematic viscosity of water. Three-dimensional (3D) instantaneous velocities were measured using a 16 MHz Micro ADV system, manufactured by Sontek. The measurement time and frequency were set as 60 s and 50 Hz, respectively, at each measuring point. Figure 3 displays arrangement of measuring points along cross section; seven vertical lines were measured across the section, where the mixing layer was confirmed to be fully developed. The vertical interval was 1–2 cm; for zones near the channel's bottom and water surface, a finer 0.5 cm interval was applied.

5 Results

This study compared data from three models (HM, SFM, and MLM) against experimental data for the lateral distribution of depth-averaged longitudinal velocity in channels with unevenly distributed vegetation. Manning's roughness coefficient and dimensionless eddy viscosity coefficient used in the models were listed in Table 2. The values of \bar{K} in each model were displayed in Table 3. Figure 4 showed the results of cases A1 and B4.

The steep gradient at the interface between the vegetated and non-vegetated zone ($y = 0.3$ m) verified that significant mass and momentum exchange occurs. However, all three models overestimated U_d at the mixing region, without considering experimental uncertainty of velocity measurements. HM generated the poorest prediction of the three models. The peak value predicted by SFM was slightly deflected to the non-vegetated region compared with the experimental data. Finally, the MLM slightly overestimated the

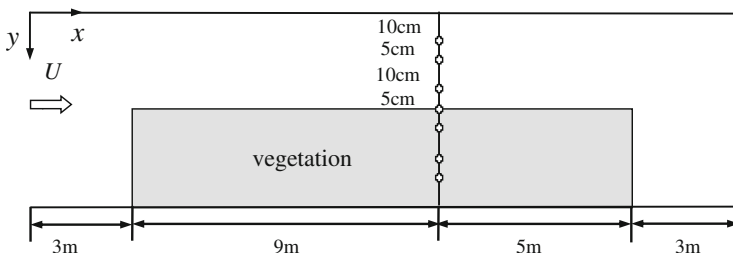
**Fig. 3** Arrangement of measuring points along cross-section

Table 2 Manning’s roughness coefficient and dimensionless eddy viscosity coefficient

	A1	A2	B1	B2	B3	B4	B5
n	0.01	0.01	0.015	0.01	0.017	0.017	0.016
f	0.017	0.016	0.039	0.018	0.046	0.052	0.044
ζ_{nv}	0.25	0.12	0.26	0.20	0.32	0.34	0.26
ζ_v	0.12	0.08	0.09	0.10	0.10	0.12	0.10

Table 3 The values of \bar{K} in the main channel and floodplain used for all cases

Cases	SFM		MLM	
	\bar{K}_{nv}	\bar{K}_v	\bar{K}_2	\bar{K}_3
A1	−0.005	0.000	−0.005	−0.002
A2	−0.005	0.002	−0.010	0.006
B1	−0.006	0.006	−0.020	−0.010
B2	−0.020	0.002	−0.010	−0.004
B3	−0.020	0.000	−0.020	0.000
B4	−0.010	−0.010	−0.010	−0.080
B5	−0.010	−0.006	−0.024	−0.004

velocity in the interface between the vegetated and non-vegetated zone, and underestimated the velocity near the channel wall in most cases.

To quantify prediction accuracy, the Root-Mean-Square Error (*RMSE*) between the modelled velocity and measured velocity was used:

$$RMSE = \sqrt{\frac{\sum_{i=1}^n ((U_d)_{ai} - (U_d)_{mi})^2}{n}} \tag{10}$$

In this expression, subscripts *a* and *m* indicate the modelled result and measured result, respectively, and *n* is the number of measured points for each case. Table 4 lists the corresponding values for all cases analyzed using the three different models; these data show that MLM generates the best prediction of the experimental data. MLM resulted in an averaged *RMSE* of 0.010 m s^{−1}; the *RSME* for HM and SFM were 0.018 m s^{−1} and 0.014 m s^{−1}, respectively.

Figure 4 and Table 4 show that Case B4 calculations using the MLM agreed most closely with the experimental data. When the aspect ratio increased, the prediction precision improved, and Case B4 had the highest aspect ratio ($\beta = 5.17$). This suggests that MLM predictions will be the most accurate in the wide and shallow channels, and the sidewall effect can be ignored when studying these areas.

6 Discussions

6.1 Parameter \bar{K}

Rameshwaran and Shiono [10] documented significant secondary flow in the mixing region; its intensity increased as the relative water depth increased. Therefore, it was not

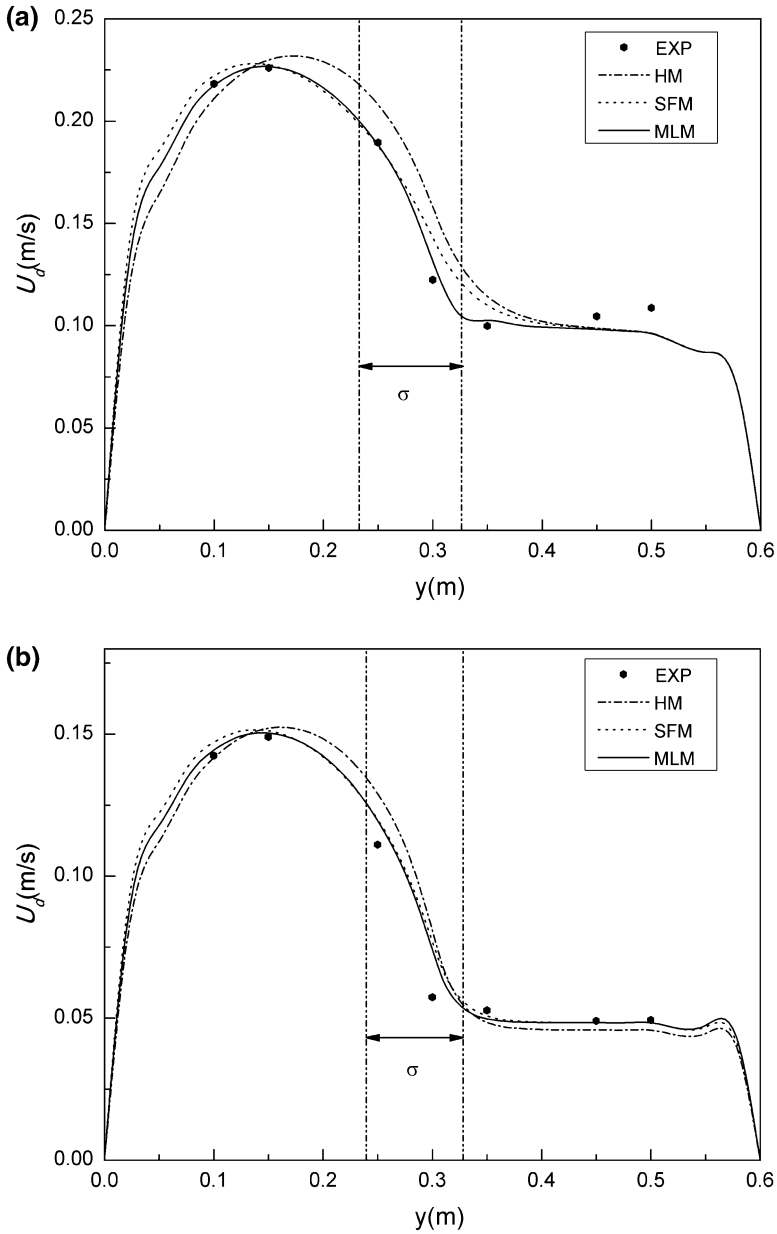


Fig. 4 Comparison between analytical and experimental U_d (case A1 (a) and B4 (b))

surprising that the model worked well when introducing the effect of secondary flow for the seven cases having a high relative water depth ($H_r \geq 0.61$). Ervine et al. [5] suggested the K would be equal or less than 0.5 % for straight channels; however, in this study, \bar{K} varied from -0.024 to 0.006 . This difference may be caused by the relative depth, and the influence of rough submerged vegetation on secondary circulation. This latter impact was also found by Ohmoto et al. [34] when studying a channel with vegetation at one side. In

Table 4 The *RMSE* for all cases

	<i>RMSE</i> (m s ⁻¹)						
	A1	A2	B1	B2	B3	B4	B5
HM	0.018	0.026	0.016	0.018	0.017	0.013	0.016
SFM	0.011	0.019	0.013	0.015	0.014	0.009	0.014
MLM	0.008	0.013	0.010	0.011	0.012	0.007	0.011

that study, the secondary flow intensity was stronger when there was submerged vegetation than when there was emergent vegetation. Furthermore, the secondary flow cell pattern was controlled by the shape of the cross section and its roughness distribution. Knight et al. [35] suggested that the signs of \bar{K} should be alternated, coupled, and related to the rotation direction of secondary cells. A more accurate prediction can be expected once proper values were adopted. From Fig. 4, it was not difficult to find that the better prediction can be made, if the sign of \bar{K} for four sub-areas in MLM were (+, -, -, +), accordingly, which were consistent with the work of Knight.

6.2 Drag coefficient C_D

Figure 5 shows the relationship between C_D and Re_v (varied from 46.82 to 156.73), where C_D is used to model the seven cases. C_D increased when the depth-averaged velocity decreased; this finding was similar to findings from Tanino et al. [36] and Kothyari et al. [37]. A sensitivity analysis also investigated the effect of C_D on the prediction (Fig. 6). The values of C_D were set as 0.5 C_D , 1.0 C_D , 1.5 C_D , and 2.0 C_D . The results indicated that the

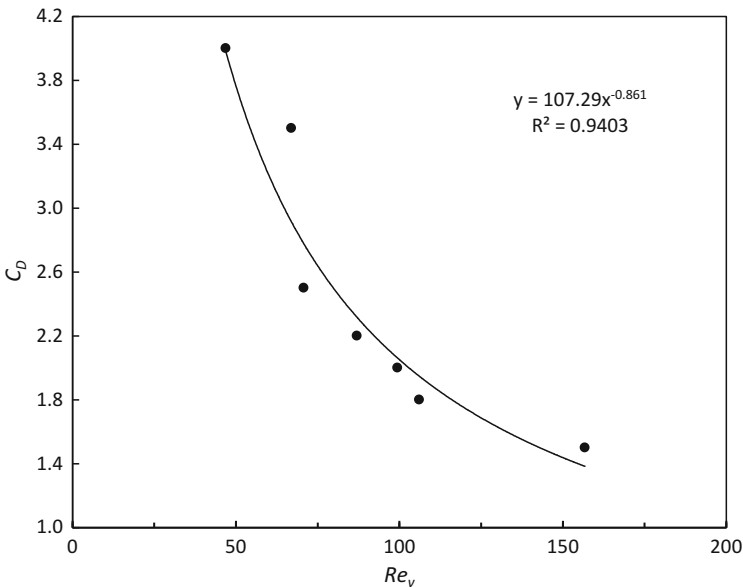


Fig. 5 Re_v versus C_D used for the seven cases

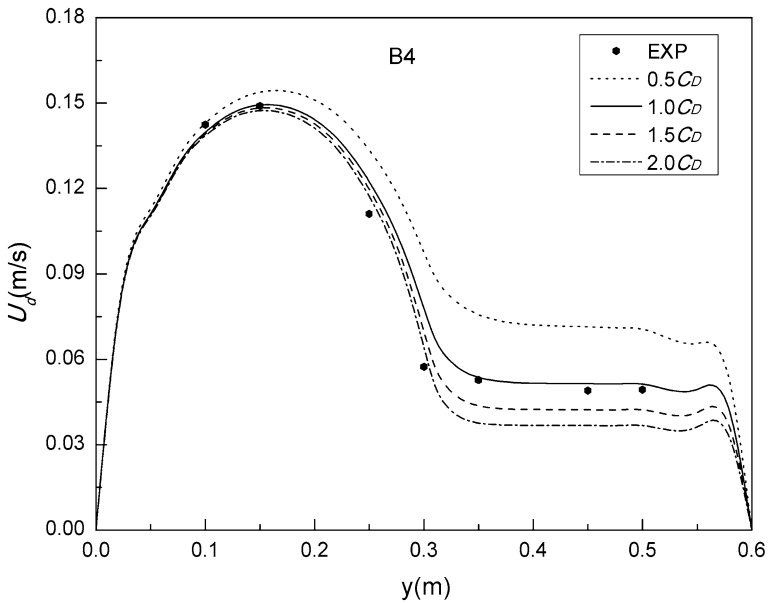


Fig. 6 Sensitivity analysis of drag coefficient C_D by MLM

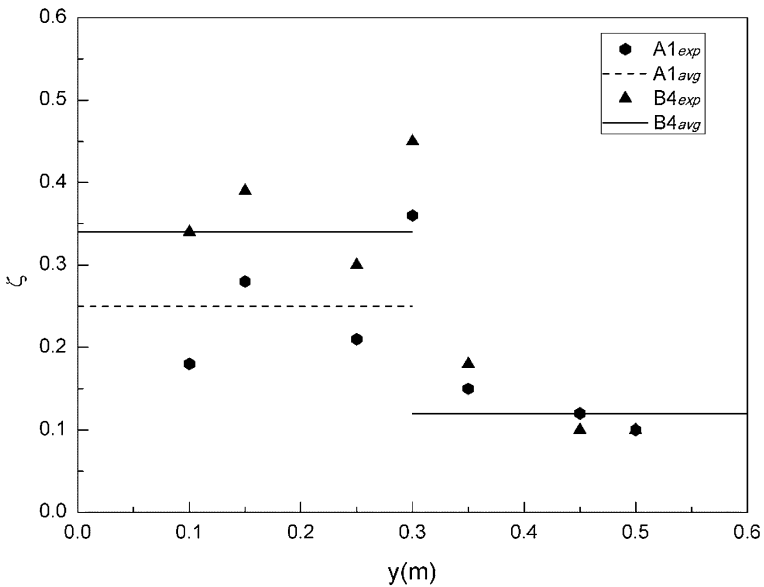


Fig. 7 Dimensionless eddy viscosity for case A1 and B4

drag coefficient C_D significantly influenced the lateral distribution of streamwise velocity in the vegetated region. As such, good estimates were not possible until proper values were adopted.

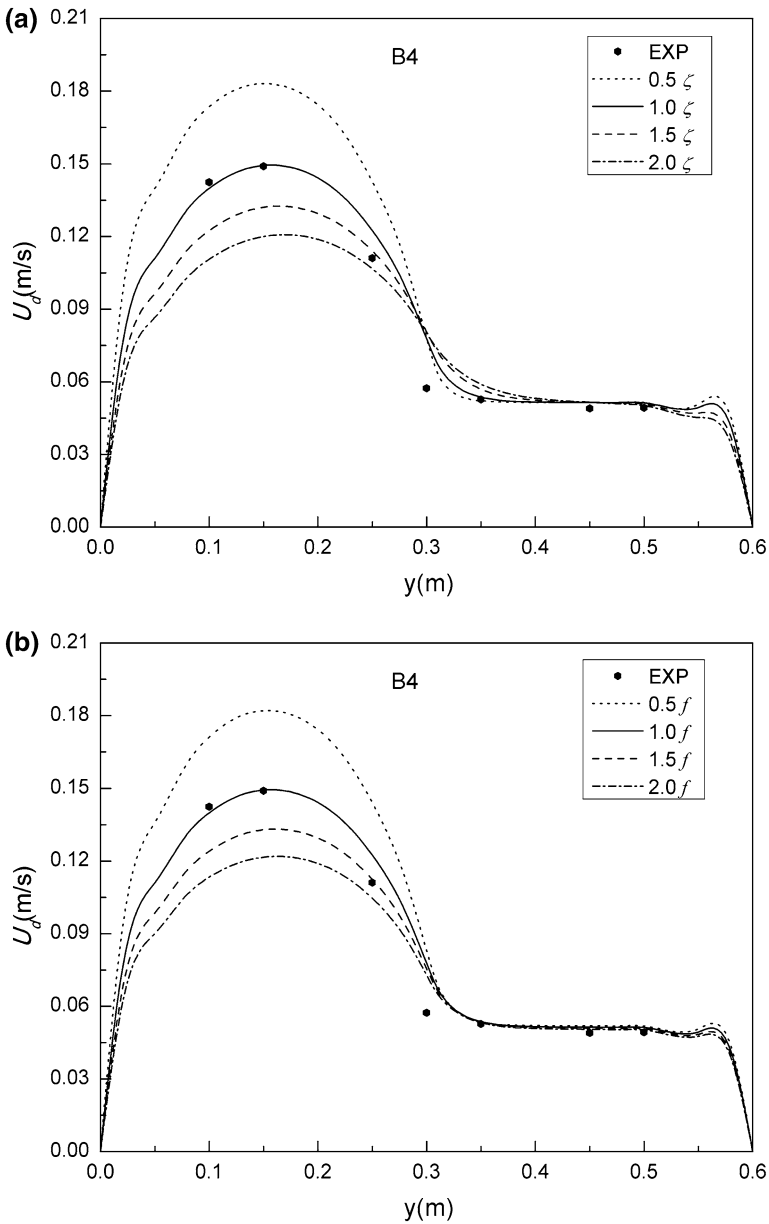


Fig. 8 Influence of dimensionless eddy viscosity (a) and Darcy-Weisbach factor (b) on the calculated U_d

6.3 Eddy viscosity ζ and Darcy-Weisbach factor f

In this experiment, the instantaneous and the temporal averaged velocity in x, y, z directions were measured to facilitate calculation of Reynolds stresses. Figure 7 shows the dimensionless eddy viscosity, determined using equations $\overline{\tau_{yx}} = -\rho \overline{u'v'} = \rho \epsilon_{xy} \frac{\partial U_d}{\partial y}$ and

$\overline{e_{xy}} = \zeta HU^*$, in which $U^* = \sqrt{gRS_0}$. The local velocity gradient, $\partial U_d / \partial y$, was estimated using a third-order polynomial best fit across five consecutive data points. Results show that ζ_{nv} is larger than ζ_v , because of the high relative water depth ($Hr \geq 0.61$). This finding is consistent with Fernandes et al. [38], whose research shows that the dimensionless eddy viscosity coefficient in a floodplain decreases as water depth increases.

The sensitivity analysis also considered the dimensionless eddy viscosity coefficient ζ and Darcy-Weisbach factor f using MLM, presented in Fig. 8. The values of ζ and f were set as 0.5ζ , 1.0ζ , 1.5ζ , 2.0ζ , and $0.5 f$, $1.0 f$, $1.5 f$, $2.0 f$, respectively. The results indicated that both dimensionless eddy viscosity and the Darcy-Weisbach factor played a significant role in the lateral distribution of streamwise velocity. As ζ or f increased, the velocity decreased, whereas the velocity in the non-vegetated region gradually reached a constant at a relatively high ζ or f . These factors were not sensitive to vegetation. Therefore, this study concludes that the effect of ζ cannot be ignored in a non-vegetated region, which is different from conclusions proposed by Zeng et al. [24] and Liu et al. [15]. For the cases in this study, the transverse shear was obvious in non-vegetated areas.

7 Conclusions

In this study, three models, the huai model (HM), secondary flow model (SFM), and mixing layer model (MLM), were adopted to investigate the physical mechanisms and critical parameters affecting velocity in a rectangular channel with laterally unevenly distributed vegetation. This included modelling solutions for the lateral distribution of depth-averaged streamwise velocity, including examining flow feature parameters, such as bed friction factor, dimensionless eddy viscosity, secondary flow coefficient, and vegetation drag coefficient.

Comparison of the modelled solutions and experimental data indicated that the MLM resulted in the most precise prediction of the three models. This was particularly true for the wide and shallow channels, because of the clear three-dimensional flow features and prominent secondary flow cells in the mixing region. A regression analysis was used to assess the relationship between the vegetation drag coefficient C_D and vegetation Reynolds number Re_v in channels with submerged vegetation. In addition, a sensitivity analysis indicated that the dimensionless eddy viscosity ζ cannot be ignored, as it influenced velocity distribution in a similar way as the bed friction factor. Although the MLM, based on the mixing region concept, worked well, there were many and varied methods to determine the range of mixing region, pointing to the need for further study about mixing mechanisms.

Acknowledgments This work was supported in part by the natural science foundation of China (No. 51379154, 51439007 and 11472199).

References

- Stephenson D, Kolovopoulos P (1990) Effects of momentum transfer in compound channels. *J Hydraul Eng* 116(12):1512–1522. doi:10.1061/(Asce)0733-9429(1990)116:12(1512)
- Shiono K, Knight DW (1988) Two dimensional analytical solution for a compound channel. Proceedings. 3rd International Symposium on Refined Flow Modelling and Turbulence Measurements, Tokyo, pp 503–510

3. Shiono K, Knight DW (1990) Mathematical models of flow in two or multi stage straight channels. Proceedings of International Conference on River Flood Hydraulics: pp 229–238
4. Shiono K, Knight DW (1991) Turbulent open channel flows with variable depth across the channel. *J Fluid Mech* 222:617–646. doi:[10.1017/S0022112091001246](https://doi.org/10.1017/S0022112091001246)
5. Ervine DA, Babaeyan-Koopaei K, Sellin RHJ (2000) Two-dimensional solution for straight and meandering overbank flows. *J Hydraul Eng* 126(9):653–669. doi:[10.1061/\(Asce\)0733-9429\(2000\)126:9\(653\)](https://doi.org/10.1061/(Asce)0733-9429(2000)126:9(653))
6. Omran M, Knight DW, Beaman F, Morvan H (2008) Modelling equivalent secondary current cells in rectangular channels. *River Flow* 1:75–82
7. Tang XN, Knight DW (2009) Analytical models for velocity distributions in open channel flows. *J Hydraul Res* 47(4):418–428. doi:[10.3826/jhr.2009.3187](https://doi.org/10.3826/jhr.2009.3187)
8. van Prooijen BC, Battjes JA, Uijttewaai WSJ (2005) Momentum exchange in straight uniform compound channel flow. *J Hydraul Eng* 131(3):175–183. doi:[10.1061/\(Asce\)0733-9429\(2005\)131:3\(175\)](https://doi.org/10.1061/(Asce)0733-9429(2005)131:3(175))
9. Tang XN, Knight DW (2008) Lateral depth-averaged velocity distributions and bed shear in rectangular compound channels. *J Hydraul Eng* 134(9):1337–1342. doi:[10.1061/\(Asce\)0733-9429\(2008\)134:9\(1337\)](https://doi.org/10.1061/(Asce)0733-9429(2008)134:9(1337))
10. Rameshwaran P, Shiono K (2007) Quasi two-dimensional model for straight overbank flows through emergent vegetation on floodplains. *J Hydraul Res* 45(3):302–315
11. Huai WX, Xu ZG, Yang ZH, Zeng YH (2008) Two dimensional analytical solution for a partially vegetated compound channel flow. *Appl Math Mech-Engl* 29(8):1077–1084. doi:[10.1007/s10483-008-0811-y](https://doi.org/10.1007/s10483-008-0811-y)
12. Huai WX, Geng CA, Zeng YH, Yang ZH (2011) Analytical solutions for transverse distributions of stream-wise velocity in turbulent flow in rectangular channel with partial vegetation. *Appl Math Mech* 32(4):459–468. doi:[10.1007/s10483-011-1430-6](https://doi.org/10.1007/s10483-011-1430-6)
13. Chen G, Huai WX, Han J, Zhao MD (2010) Flow structure in partially vegetated rectangular channels. *J Hydrodyn* 22(4):590–597. doi:[10.1016/S1001-6058\(09\)60092-5](https://doi.org/10.1016/S1001-6058(09)60092-5)
14. de Lima AC, Izumi N (2014) Linear stability analysis of open-channel shear flow generated by vegetation. *J Hydraul Eng* 140(3):231–240. doi:[10.1061/\(Asce\)Hy.1943-7900.0000822](https://doi.org/10.1061/(Asce)Hy.1943-7900.0000822)
15. Liu C, Luo X, Liu XN, Yang KJ (2013) Modeling depth-averaged velocity and bed shear stress in compound channels with emergent and submerged vegetation. *Adv Water Resour* 60:148–159. doi:[10.1016/j.advwatres.2013.08.002](https://doi.org/10.1016/j.advwatres.2013.08.002)
16. Stone BM, Shen HT (2002) Hydraulic resistance of flow in channels with cylindrical roughness. *J Hydraul Eng* 128(5):500–506. doi:[10.1061/\(Asce\)0733-9429\(2002\)128:5\(500\)](https://doi.org/10.1061/(Asce)0733-9429(2002)128:5(500))
17. Spooner J, Shiono K (2003) Modelling of meandering channels for overbank flow. *Proc Ins Civ Eng-Water Marit Eng* 156(3):225–233
18. Kincaid DR, Cheney E (2002) Numerical analysis: mathematics of scientific computing, 3rd version. American Mathematical Society, Providence
19. Jarvela J (2002) Flow resistance of flexible and stiff vegetation: a flume study with natural plants. *J Hydrol* 269(1–2):44–54. doi:[10.1016/S0022-1694\(02\)00193-2](https://doi.org/10.1016/S0022-1694(02)00193-2)
20. Wilson CAME (2007) Flow resistance models for flexible submerged vegetation. *J Hydrol* 342(3–4):213–222. doi:[10.1016/j.jhydrol.2007.04.022](https://doi.org/10.1016/j.jhydrol.2007.04.022)
21. Sharifi S, Sterling M, Knight DW (2009) A novel application of a multi-objective evolutionary algorithm in open channel flow modelling. *J Hydroinform* 11(1):31–50. doi:[10.2166/hydro.2009.033](https://doi.org/10.2166/hydro.2009.033)
22. Myers WRC, Knight DW, Lyness JF, Cassells JB, Brown F (1999) Resistance coefficients for inbank and overbank flows. *Proc Ins Civ Eng-Water Marit Eng* 136(2):105–115
23. Xu WL, Knight DW, Tang XN (2004) Study on friction factor and eddy viscosity of overbank flows. *Adv Water Sci* 15(6):723–727 (in Chinese)
24. Zeng YH, Guymer I, Spence KJ, Huai WX (2012) Application of analytical solutions in trapezoidal compound channel flow. *River Res Appl* 28(1):53–61. doi:[10.1002/rra.1433](https://doi.org/10.1002/rra.1433)
25. Lambert MF, Sellin RHJ (1996) Discharge prediction in straight compound channels using the mixing length concept. *J Hydraul Res* 34(3):381–394
26. Hirschowitz PM, James CS (2009) Transverse velocity distributions in channels with emergent bank vegetation. *River Res Appl* 25(9):1177–1192. doi:[10.1002/rra.1216](https://doi.org/10.1002/rra.1216)
27. Choi SU, Joung Y (2012) Numerical prediction of morphological change of straight trapezoidal open-channel. *J Hydro-Environ Res* 6(2):111–118. doi:[10.1016/j.jher.2012.01.003](https://doi.org/10.1016/j.jher.2012.01.003)
28. Knight DW (1999) Flow mechanisms and sediment transport in compound channels. *Int J Sediment Res* 14(2):217–236
29. Kouwen N, Unny TE, Hill HM (1969) Flow retardance in vegetated channel. *J Irr Drain Div* 95(IR2):329–340

30. Aberle J, Jarvela J (2013) Flow resistance of emergent rigid and flexible floodplain vegetation. *J Hydraul Res* 51(1):33–45. doi:[10.1080/00221686.2012.754795](https://doi.org/10.1080/00221686.2012.754795)
31. Chapman JA, Wilson BN, Gulliver JS (2015) Drag force parameters of rigid and flexible vegetal elements. *Water Resour Res* 51(5):3292–3302. doi:[10.1002/2014WR015436](https://doi.org/10.1002/2014WR015436)
32. Tsujimoto T, Okada T, Kontani K (1993) Turbulent structure of open channel flow over flexible vegetation. KHL Progressive Report 4. Kanazawa University, Kanazawa, Japan
33. Meijer DG (1998) Model test submerged vegetation, physical model investigation. Report of HKV Consultants, Rijkswaterstaat/RIZA, Den Haag [in Dutch]
34. Ohmoto T, Okamoto T, Nakashima T (2002) Three-Dimensional Flow Structure in an Open Channel with a Flexible Vegetation Zone. In: *Hydraulic Measurements and Experimental Methods 2002*. American Society of Civil Engineers, pp 1–10
35. Knight DW, Omran M, Tang XN (2007) Modeling Depth-Averaged Velocity and Boundary Shear in Trapezoidal Channels with Secondary Flows. *J Hydraul Eng* 133:39–47. doi:[10.1061/\(Asce\)0733-9429\(2007\)133:1\(39\)](https://doi.org/10.1061/(Asce)0733-9429(2007)133:1(39))
36. Tanino Y, Nepf HM (2008) Laboratory investigation of mean drag in a random array of rigid, emergent cylinders. *J Hydraul Eng* 134(1):34–41. doi:[10.1061/\(Asce\)0733-9429\(2008\)134:1\(34\)](https://doi.org/10.1061/(Asce)0733-9429(2008)134:1(34))
37. Kothiyari UC, Hayashi K, Hashimoto H (2009) Drag coefficient of unsubmerged rigid vegetation stems in open channel flows. *J Hydraul Res* 47(6):691–699. doi:[10.3826/jhr.2009.3283](https://doi.org/10.3826/jhr.2009.3283)
38. Fernandes JN, Leal JB, Cardoso AH (2014) Improvement of the Lateral Distribution Method based on the mixing layer theory. *Adv Water Resour* 69:159–167. doi:[10.1016/j.advwatres.2014.04.003](https://doi.org/10.1016/j.advwatres.2014.04.003)